Theor Chem Acc (2006) 115: 205–211
DOI 10.1007/s00214-005-0064-2

REGULAR ARTICLE

Chaoyang Wang · Yue Zhang · Shaowen Zhang
Qian Shu Li

Direct ab initio dynamics study for the hydrogen abstraction reaction: $CH_2(^3B_1) + H_2CO \rightarrow CH_3 + CHO$

Received: 28 July 2004 / Accepted: 28 April 2005 / Published online: 21 December 2005
© Springer-Verlag 2005

Abstract We present a direct ab initio dynamics study of thermal rate constants of the hydrogen abstraction reaction of $CH_2(^3B_1) + H_2CO \rightarrow CH_3 + CHO$. The MP2/cc-pVDZ method is employed to optimize the geometries of stationary points as well as the points on the minimum energy path. The energies of all the points were further refined at the CCSD(T)/cc-pVTZ level of theory based on the Moller–Plesset perturbation theory (MP2) optimized geometries. The rate constants were evaluated using the conventional transition state theory, the canonical variational TST, and the improved canonical variational TST, also both including small-curvature tunneling correction in the temperature range of 300–2,500 K. The calculated results show that the rate constants have positive temperature dependence in the calculated temperature range. The calculated results show that the tunneling effect is important at low temperature region.

Keywords Direct ab initio dynamics · Variational transition state theory · Small-curvature tunneling · Rate constant · Formaldehyde

1 Introduction

The Methylene radical [$CH_2(^3B_1)$] is a key intermediate in hydrocarbon combustion reaction and atmospheric processes. Up to now, a number of theoretical and experimental investigations have been performed on the $CH_2(^3B_1)$ reaction with atoms, radicals and molecules such as H_2 [1,2], C_2H_2 [3,4], CH_3 [5,6], CO [7], O_2 [8], NO [9], O [10], H_2CO [7,11] etc. Furthermore, it is well known that formaldehyde molecule (H_2CO) in the gas phase are widespread in atmospheric and combustion processes. Thus the reaction of $CH_2(^3B_1)$ with H_2CO might influence the decay rate of the $CH_2(^3B_1)$ radical and might have further effect on the other chain reactions considered in combustion processes.

In spite of its importance in combustion and atmospheric chemistry, this kinetic behaviors of the reaction of $CH_2(^3B_1)$ radical with H_2CO molecule has not been experimentally studied to the best of our present knowledge due to the difficulties in experimental techniques. Theoretically, Tsang and Hampson [7] had investigated the rate constant of the title reaction using the bond energy and bond order (BEBO) method and gave an upper limit value of the reaction rate constant $k = 1.0 \times 10^{-14}$ cm^3 mol^{-1} s^{-1} over the temperature range of 300–2,500 K. To better understand its kinetic mechanism of the reaction of $CH_2(^3B_1)$ radical with H_2CO molecule in the course of combustion and atmosphere, high-level ab initio calculation and rate constants calculation are still required.

The objective of this study is to accurately calculate the rate constants of the reaction $CH_2(^3B_1) + H_2CO \rightarrow CH_3 + CHO$. The thermal rate constants of the title reaction are calculated using the CVT [canonical variational transition state theory (TST)] [12–15], the CVT with the small-curvature tunneling (SCT) [14,16] correction (CVT/SCT), the improved canonical variational TST (ICVT), the ICVT with the SCT correction (ICVT/SCT) based on the direct ab initio dynamics approaches [17,18].

2 Computational methods

2.1 Electronic calculations

All the electronic structure calculations are carried out with the program package GAUSSIAN 98 [19]. The geometries and harmonic vibrational frequencies of all stationary points (the reactants, transition state and products) are calculated

C. Wang (✉)
School of Chemistry and Environment,
South China Normal University,
Guangzhou, 510631, Peoples Republic of China

Y. Zhang
Department of Chemistry, Shijiazhuang College,
Shijiazhuang, 050036, Peoples Republic of China

Y. Zhang · S. Zhang · Q.S. Li
School of science, Beijing Institute of Technology,
Beijing, 100081, Peoples Republic of China
E-mail: chaoyangwang111@yahoo.com.cn

using second-order Moller–Plesset perturbation theory [20] (MP2) with the Dunning's [21,22] correlation consistent basis set including double-zeta, namely, cc-pVDZ. It is well known that the MP2 energies for many species are generally inaccurate due to the nature of the method, particularly for radical. Thus, the energies of the projected Moller–Plesset perturbation theory (PMP2) are adopted to obtain relative accurate results. To improve the accuracy of the energetics, single-point calculations for all the stationary points and the selected points along the minimum energy path (MEP) are carried out at the CCSD(T)/cc-pVTZ level of theory using the MP2/cc-pVDZ optimized geometries. Here the CCSD(T)/cc-pVTZ are referred to as the coupled cluster calculation including single and double substitutions with a triples contribution to the energy added [23], using Dunning's correlation consistent polarized valence triple-zeta basis set. For convenience, we denote the single-point energy results as the CCSD(T)//MP2. The IRC is calculated in mass-weighted Cartesian coordinates with a gradient step size of 0.01 $(\text{amu})^{1/2}$ bohr using Gonzalez–Schlegel method [24] at the MP2/cc-pVDZ level of theory. Also, the energy derivatives, including gradients and Hessians at along the MEP, are obtained at the same level of theory. The potential energy curve is further refined at the CCSD(T)/cc-pVTZ level of theory based on IRC curve at the MP2 level of theory.

2.2 Rate constants

The thermal rate constants at various temperatures are calculated using conventional TST, CVT and ICVT as implemented in Polyrate8.2 program [25]. The CVT thermal rate constants for the gas-phase bimolecular reaction is determined by varying the location of the dividing surface along the reaction coordinate, s, to minimize the generalized TST rate constants, $k^{\mathrm{GT}}(T,s)$. Thus the CVT thermal rate constants, $k^{\mathrm{CVT}}(T,s)$, at temperature T is given by

$$k^{\mathrm{CVT}}(T) = \min\left\{k^{\mathrm{GT}}(T,s)\right\} = \min\left\{\sigma\frac{k_{\mathrm{B}}T}{h}\frac{Q^{\mathrm{GT}}(T,s)}{Q^{\mathrm{R}}(T)} \exp\left[-V_{\mathrm{MEP}}(s)/k_{\mathrm{B}}T\right]\right\} \quad (1)$$

where QGT is the internal partition function of the generalized transition state; QR is the reactant partition function per unit volume; σ is the symmetry factor, which is 4 for the forward and 4 reverse direction of the $CH2(^3B_1) + H2CO \rightarrow CH3 + CHO$ reaction; and k_{B} and h are Boltzmann's and Plank's constants, respectively. Q^{GT} and Q^{R} are approximated as the products of electronic, rotational, and vibrational partition functions. For bimolecular reactions, the relative translational partition function per unit volume is calculated classically. Translational and rotational partition functions are evaluated classically whereas the vibrational partition functions were calculated quantum mechanically within the harmonic approximation.

The ICVT thermal rate constants, $k^{\mathrm{ICVT}}(T)$, is used in order to treat the threshold region as accurately as microcanonical variational theory. The expression is written

$$k^{\mathrm{ICVT}}(T) = \left(\frac{k_{\mathrm{B}}T}{h}\right)K^{\neq,0}\min_{s} \times\left\{\exp\left[-\Delta G^{\mathrm{IGT}}(T,s)/kT\right]\right\} \quad (2)$$

where k_{B} is Boltzmann's constant, T is the temperature, h is Planck's constant, $K^{\neq,0}$ is the reciprocal of the standard state concentration, s denotes a point along the MEP, $\Delta G^{\mathrm{IGT},0}(T,s)$ is the standard-state improved generalized free energy of activation at temperature T for the generalized transition state located at s, and R is the gas constant.

Furthermore, the CVT and ICVT rate constants are corrected with the SCT transmission coefficient. The SCT transmission coefficients, that include the reaction-path curvature effect on the transmission probability, are based on the centrifugal-dominant small-curvature semiclassical adiabatic ground-state (CD-SCSAG) approximation. In particular, the transmission probability at energy E is given by

$$P(E) = \frac{1}{\{1+\mathrm{e}^{-2\theta(E)}\}} \quad (3)$$

where $\theta(E)$ is the imaginary action integral evaluated along the reaction coordinate

$$\theta(E) = \frac{2\pi}{h}\int_{s_{\mathrm{l}}}^{s_{\mathrm{r}}}\sqrt{2\mu_{\mathrm{eff}}(s)\left|E - V_a^{\mathrm{G}}(s)\right|}ds \quad (4)$$

and where the integration limits s_{l} and s_{r} are the reaction coordinate classical turning points. The reaction-path curvature effect on the tunneling probability is included in the effective reduced mass μ_{eff}.

$$\mu_{\mathrm{eff}}(s) = \mu[M(s)]^2 \quad (5)$$

where $M(s)$ is a metric factor.

3 Results and discussion

3.1 Stationary points

Pictorial of optimized geometric parameters of the stationary points at the MP2/cc-pVDZ level of theory along with the available experimental values are shown in Fig. 1. It can be seen that the calculated results are in good agreement with the available experimental data [26,27]. The largest deviation of the bond length and the bond angle are 0.11 Å for C–O of H_2CO and 1.3° for ∠HCH of H_2CO, respectively. It is obvious that the 0.11 Å deviation between theory and experiment for the C–O bond length in H_2CO molecule is large at the MP2 level of theory. To explain the situation clearly, the MPW1K/6-31+G(d,P) method proposed by Truhlar and co-workers is adopted to compute the geometries of H_2CO molecule. The C–O bond length, C–H bond length, and ∠OCH bond angle are 1.196 Å, 1.099 Å, and 121.8° at the MPW1K/6-31+G(d,P) level of theory, respectively,

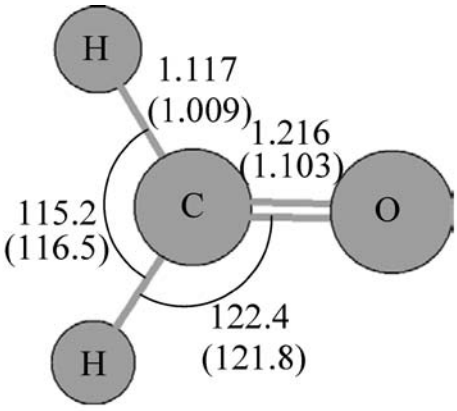

HCHO (C_{2v})

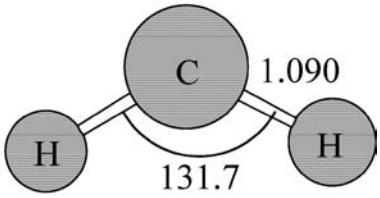

CH_2 (C_{2v})

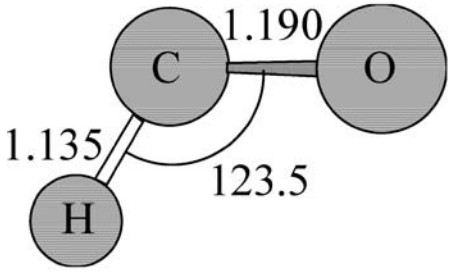

CHO (Cs)

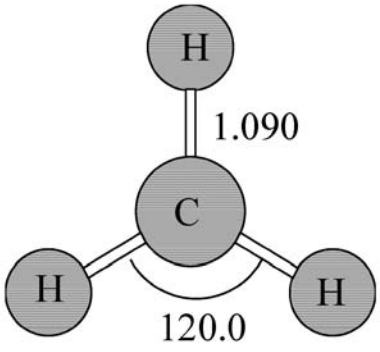

CH_3 (D_{3h})

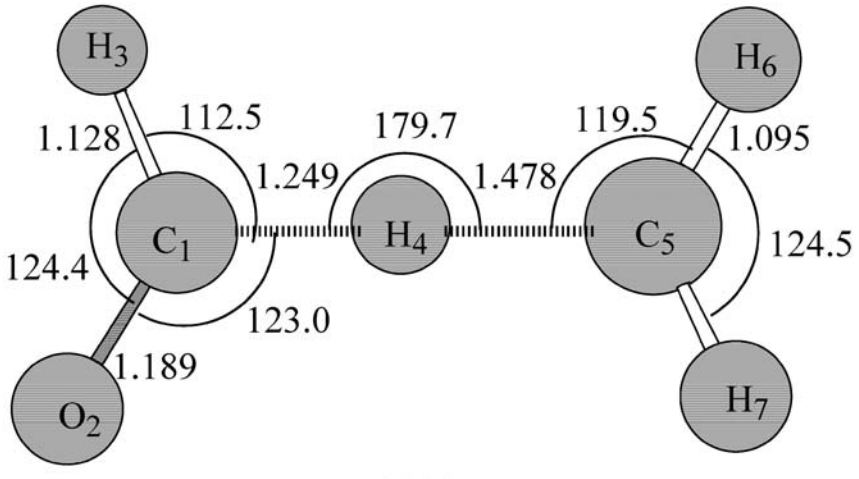

TS (Cs)

Fig. 1 Pictorial of optimized geometries [the bond distance in Å bond angle in degrees) of the stationary points at the MP2/cc-pVDZ level of theory. The *numbers in the parenthesis* are the experimental values

which are very closer to the corresponding experimental values. The relatively large deviation between the experiment and MP2 theory might result from that the electronic distribution cannot be correctly described at the MP2 level of theory; Meanwhile the MPW1K/6-31+G(d,P) method gives good description for H_2CO molecule. As a matter of fact, the MPW1K/6-31+G(d,P) method has widely been applied in kinetic calculations. For the transition state, the breaking H_4–C_5 bond distance is elongated by 11.8% at the MP2/cc-pVDZ level of theory compared to the reactant (H_2CO), and the forming C_1–H_4 bond distance is elongated by 31% with respect to the product (CH_3) at the same level of theory. This means that the transition state structure is more reactant-like than product-like, and the reaction will proceed via early transition state. This is the expected behavior from Hammond's postulate for exothermic reactions.

Table 1 lists the harmonic vibrational frequencies and zero-point energies of reactants, products and transition state at the MP2/cc-pVDZ level of theory along with the available experimental data [28–31]. From Table 1, one can find that the calculated frequencies at the MP2/cc-pVDZ level of theory are consistently larger than the corresponding experimental values [28–31]. However, the discrepancies between theoretical results and experimental data are generally within 7%. This shows that the calculated frequencies are in agreement with the available experimental values. After the calculated frequencies are scaled by a factor of 0.9499 (Refer to web site:www.nist.gov), the corresponding difference between theory and the available experiment becomes smaller. For the transition state, the character of the stationary point is conformed by normal mode analysis, which yields one and only one imaginary frequency (1,768 cm^{-1}) whose eigen vector corresponds to the direction of the reaction.

Table 1 The harmonic vibrational frequencies (cm^{-1}) and zero-point energies (kcal mol^{-1}) of reactants, products and transition state at the MP2/cc-pVDZ level of theory

Species	Frequencies	ZPE
$CH_2(C_{2v})$	1,159, 3,206, 3,439	11.16
$H_2CO(C_{2v})$	1,199, 1,275, 1,547, 1,783, 2,965, 3,034 (1,139, 1,211, 1,469, 1,694, 2,816, 2,881)	16.87
Experiment[a]	1,167, 1,249, 1,500, 1,746, 2,783, 2,843	
$CH_3(D_{3h})$	383, 1,428, 1,428, 3,179, 3,384, 3,384 (364, 1,356, 1,356, 3,019, 3,214, 3,214)	18.85
Experiment[b]	1,372, 2,914	
CHO (C_s)	1,124, 1,943, 2,716 (1,067, 1,845, 2,580)	8.27
Experiment[c]	1,066, 1,812, 2,596	
TS(C_1)	79, 124, 274, 437, 467, 597, 1,237, 1,245, 1,311, 1,520, 2,470, 2,911, 3,166, 3,358, 1,768*i*	27.44

Note: All the experimental frequencies are anharmonic; The numbers in the parenthesis are the theoretically calculated harmonic vibrational frequencies scaled by a factor of 0.9499 (refer to web site:http://www.nist.gov)
[a]Ref. [28]
[b]Ref. [29]
[c]Ref. [30]

The reaction energetics information including the reaction energies, the reaction enthalpies, and the forward classical potential barrier heights at the PMP2/cc-pVDZ and the CCSD(T)/cc-pVTZ//MP2/cc-pVDZ levels of theory are listed in Table 2 along with the available experimental data [31]. As can be seen from Table 2, the predicted reaction enthalpies (−20.84 kcal mol^{-1}) for the reaction at the PMP2/cc-pVDZ level of theory is slightly larger than the experimental value of −19.43 kcal mol^{-1}. However, the refined reaction enthalpies (−20.06 kcal mol^{-1}) at the CCSD(T)/cc-pVTZ level of theory are much close to the experimental value. Since the calculated reaction enthalpies can be effectively improved by means of the CCSD(T) methods. Thus the CCSD(T)//MP2 method is very suitable in predicting the energies of the title reaction. With respect to the forward barrier height, the single-point calculation at the CCSD(T)//MP2 method decreases the forward barrier height including zero-point energy obtained at the PMP2/cc-pVDZ level of theory by 1.25 kcal mol^{-1}. This shows that the single-point calculation can effectively improve the accuracy of the energetics information.

3.2 Reaction path properties

The minimum energy path is determined at the MP2/cc-pVDZ level of theory using the intrinsic reaction coordinate theory [24] with a step size of 0.01 $(amu)^{1/2}$ bohr. Figure 2 shows the changes of the forming and breaking bond distances (Å) as function of the reaction coordinate s $(amu)^{1/2}$ bohr at the MP2/cc-pVDZ level of theory. From Fig. 2, for the reaction, the active H_4–C_5 (forming) and C_1–H_4 (breaking) bonds change strongly, while the remaining bond lengths are almost unchanged over the whole reaction processes. The forming bond H_4–C_5 and the breaking bond C_1–H_4 shortens and stretches linearly and rapidly from $s = -0.25$ to $s = 0.75$ $(amu)^{1/2}$ bohr, respectively. Thus, the changes of the bond lengths occur mainly in the region from −0.25 to 0.75 $(amu)^{1/2}$ bohr.

In order to obtain more accurate energetic information, the energy profile is further refined at the CCSD(T)/cc-pVTZ

Table 2 The reaction energetics parameters (kcal mol^{-1}) at the PMP2/cc-pVDZ and CCSD(T)/cc-pVTZ//MP2/cc-pVDZ levels of theory

Method	ΔE^{a}	ΔH°_{298K}	$V^{\neq b}$
PMP2/cc-pVDZ	−21.75	−20.84	7.42 (6.83)[d]
CCSD(T)/cc-pVTZ//MP2/cc-pVDZ	−20.97	−20.06	6.17 (5.58)[d]
Experiment		−19.43[c]	

[a]Reaction energy
[b]Classical barrier height
[c]Calculated from the standard heat of formation of reactant and product. (CH_2: 92.35 kcal mol^{-1} ; H_2CO: −27.70 kcal mol^{-1} ; CH_3: 34.82 kcal mol^{-1} ; CHO: 10.40 kcal mol^{-1}) [31]
[d]Tthe numbers in parenthesis are the classical barrier heights with zero-point energy correction

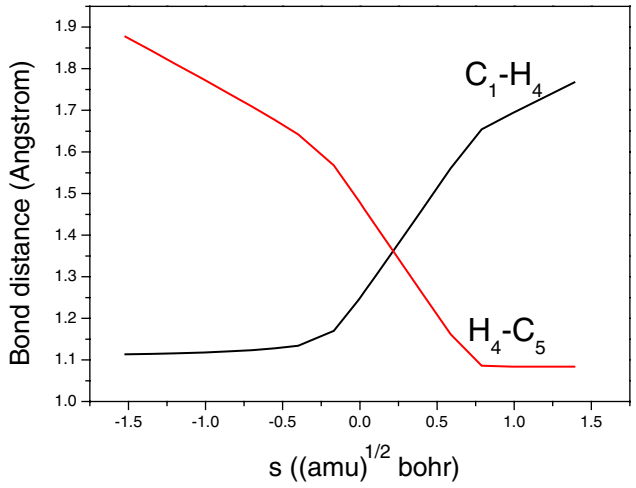

Fig. 2 Changes of the forming and breaking bond distances (Å) as a function of the reaction coordinate s ((amu)$^{1/2}$ bohr) at the MP2/cc-pVDZ level of theory

level of theory along the IRC obtained at the MP2/cc-pVDZ level of theory. The classical potential energy (V_{MEP}) and the vibrationally adiabatic ground-state potential energy (V_a^{G}) curves of the reaction as a function of reaction coordinate s ((amu)$^{1/2}$ bohr) at the CCSD(T)/cc-pVTZ//MP2/cc-pVDZ level of theory are shown in Fig. 3. As can be seen, the V_{MEP} and V_a^{G} curves are similar in shape. The position of the transition state does not greatly shift. In order to understand further the variational effect, the dynamics bottleneck properties of the title reaction based on the canonical variational transition state approach are calculated and listed in Table 3. The dynamics bottleneck properties denote the position of the variational transition state at various temperature derivates from the saddle point at $s = 0$. It can be seen from Table 3 that the largest deviation is at 1,000–2,500 K, where

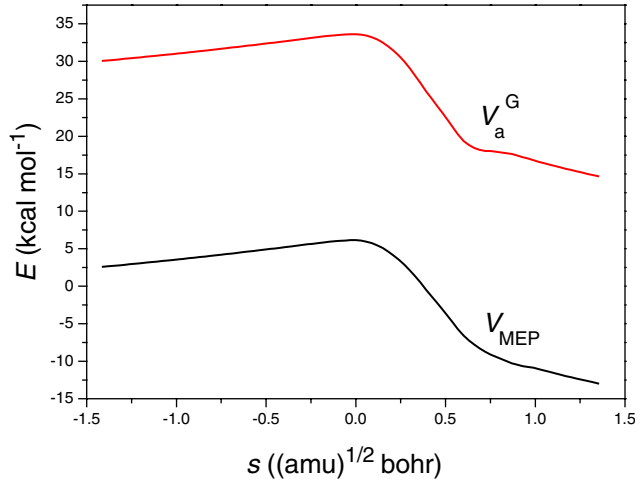

Fig. 3 The classical potential energy (V_{MEP}) and the vibrationally adiabatic ground-state potential energy (V_a^{G}) curves of the reaction as a function of reaction coordinate s((amu)$^{1/2}$ bohr) at the CCSD(T)/cc-pVTZ//MP2/cc-pVDZ level of theory

Table 3 Bottleneck properties determined using the TST and CVT methods

T (K)	s (bohr)	V_{MEP} (kcal)	V_a^{G} (kcal)
S.P.	0.000	6.17	33.62
250.00	0.004	6.17	33.62
298.00	0.004	6.16	33.62
400.00	0.004	6.16	33.62
500.00	0.005	6.16	33.62
800.00	0.005	6.16	33.62
1,000.00	0.006	6.16	33.62
1,250.00	0.006	6.16	33.62
1,500.00	0.006	6.16	33.62
2,000.00	0.006	6.16	33.62
2,500.00	0.006	6.16	33.62

$s = 0.006$ amu$^{1/2}$ bohr, corresponding V_{MEP} and V_a^{G} are 6.16 and 33.62 kcal mol^{-1}, respectively. Since for the conventional transition state ($s = 0$), V_{MEP} and V_a^{G} take values 6.17 and 33.62 kcal mol^{-1}, respectively, the largest deviations, $V_{\mathrm{MEP}}(s = 0.006) - V_{\mathrm{MEP}}(s = 0) = -0.01$ kcal mol^{-1} and $V_a^{\mathrm{G}}(s = 0.014) - V_a^{\mathrm{G}}(s = 0) = 0.00$ kcal mol^{-1}, are very small. This means that the variational corrections in the calculation of the rate constant are also very small.

3.3 Rate constant calculations

The forward rate constants calculated using CVT, ICVT, CVT/SCT and ICVT/SCT methods based on the PES information at the CCSD(T)//MP2 level of theory are shown Fig. 4. It can be seen from Fig. 4 that the rate constants have positive temperature dependence in the calculated temperature range, and the tunneling effect is important at low temperature region. The difference between the TST and CVT rate constants is quite small; i.e. 2% at 250 K and 8% at 2,500 K. At 250 K, the rate constant of ICVT/SCT is larger than that of ICVT by a factor of more than 4. As the temperature increases, the predicted rate constants become consistent with one another

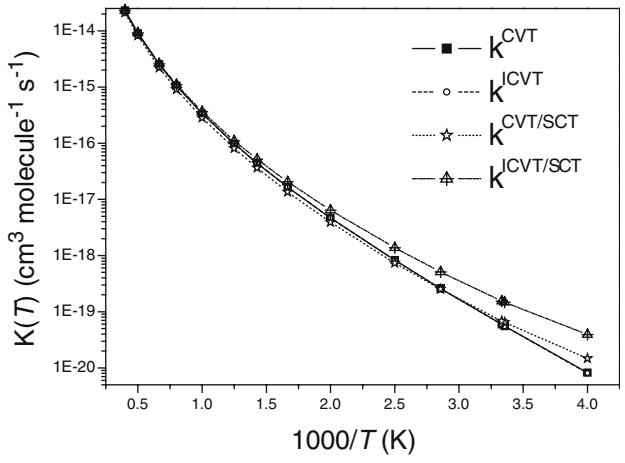

Fig. 4 Comparison of the calculated rate constants of the reaction versus $1,000/T$ at the CCSD(T)/cc-pVTZ//MP2/cc-pVDZ level of theory

Table 4 The title reaction rate constants ($cm^3\ mol^{-1}\ s^{-1}$) at the CCSD(T)/cc-pVTZ//MP2/cc-pVDZ level of theory in the temperature range 250–2,500 K

T (K)	TST	CVT	ICVT	CVT/SCT	ICVT/SCT	ICVT/SCT (hindered rotor)[a]	Ref. [7]
250.00	8.44E-21	8.25E-21	8.06E-21	4.00E-20	3.91E-20	3.31E-20	
298.00	5.71E-20	5.56E-20	5.50E-20	1.49E-19	1.47E-19	1.25E-19	
300.00	6.11E-20	5.95E-20	5.89E-20	1.57E-19	1.55E-19	1.31E-19	
350.00	2.68E-19	2.60E-19	2.58E-19	5.14E-19	5.10E-19	4.36E-19	
400.00	8.558E-19	8.26E-19	8.24E-19	1.37E-18	1.37E-18	1.24E-18	
500.00	4.86E-18	4.66E-18	4.66E-18	6.43E-18	6.43E-18	5.45E-18	
600.00	1.72E-17	1.65E-17	1.65E-17	2.06E-17	2.06E-17	1.81E-17	
700.00	4.61E-17	4.39E-17	4.39E-17	5.17E-17	5.17E-17	4.38E-17	
800.00	1.03E-16	9.74E-17	9.74E-17	1.10E-16	1.10E-16	9.63E-17	
1,000.00	3.55E-16	3.36E-16	3.36E-16	3.64E-16	3.64E-16	3.38E-16	
1,250.00	1.12E-15	1.05E-15	1.05E-15	1.10E-15	1.10E-15	9.62E-16	
1,500.00	2.68E-15	2.51E-15	2.51E-15	2.60E-15	2.60E-15	2.250E-15	
2,000.00	9.71E-15	9.06E-15	9.06E-15	9.24E-15	9.24E-15	7.93E-15	
2,500.00	2.48E-14	2.30E-14	2.30E-14	2.33E-14	2.33E-14	1.99E-14	>1.0E-14

[a]The ICVT/SCT rate constant including hindered rotor treatment

at various levels of theory. Table 4 listed the theoretical evaluated results and the other theoretical value [7]. It can be seen that the calculated rate constants are in good agreement with the literature upper limited value from Tsang et al. [7]. In addition, some frequencies at the TS are very small (79,124,274 cm^{-1}), under the situation the accuracy of the rate constants treating the method as harmonic oscillators will lower. Thus, the ICVT/SCT rate constants including hindered rotation effect were also calculated and tabulated in Table 4. It is obvious that the ICVT/SCT rate constants including the hindered rotation are close to the ICVT/SCT rate constants in the calculated temperature range, with the deviations being a factor of 1.18–1.07 at the temperature region of 250–2,500 K. The ICVT/SCT rate constants of this reaction including the hindered rotation are slightly smaller than the ICVT/SCT rate constants without hindered rotation when the temperature is above 1,250 K. Furthermore, the forward ICVT/SCT rate constants within 250–2,500 K are fitted by the three-parameter expression in units of $cm^3\ mol^{-1}\ s^{-1}$ as follows:

$$k = 1.23 \times 10^{-25} T^{4.21} e^{(-817.2/T)}$$

4 Summary

We present a direct ab initio dynamics study of thermal rate constants of the hydrogen abstraction reaction of $CH_2(^3B_1) + H2CO \rightarrow CH_3 + CHO$. The MP2/cc-pVDZ method is employed to optimize the geometries of stationary points as well as the points on the MEP. The rate constants were evaluated using the CVT, the CVT with SCT CVT/SCT, the ICVT, and the ICVT with SCT correction (ICVT/SCT) in the temperature range of 250–2,500 K. The calculated results show that the reaction rate constants have positive temperature dependence in the calculated temperature range. The calculated forward rate constants at the CCSD(T)/cc-pVTZ//MP2/cc-pVDZ level of theory are in good agreement with available literature data. Small-curvature tunneling effect is important only in low temperature range. The three-parameter fit for the reaction rate constants within 250–2,500 K is $k = 1.23 \times 10^{-25} T^{4.21} e^{(-817.2/T)}$ $cm^3\ mol^{-1}\ s^{-1}$. We hope that our kinetic studies on the direct hydrogen abstraction reaction channel may be useful for understanding the mechanism of $CH_2(^3B_1) + H_2CO$.

Acknowledgements Thanks are due to Professor D. G. Truhlar for providing the POLYRATE 8.2 program. This work was supported by National Natural Science Foundation of China (20373007) and Foundation for basic research by Beijing Institute of Technology.

References

1. Fahr A, Monks PS, Stief LJ, Laufer AH (1995) Icarus 116:415–422
2. Knyazev VD, Bencsura A, Stoliarov SI, Slagle IR (1996) J Phys Chem 100:11346–11354
3. Duran RP, Amorebieta VT, Colussi AJ (1989) Int J Chem Kinet 21:947
4. Weissman M, Benson SW (1984) Int J Chem Kinet 16:307
5. Thorn RP, Payne WA, Chillier XDF, Stief LJ, Nesbitt FL, Tardy DD (2000) Int J Chem Kinet 32:304–316
6. Fahr A, Laufer AH, Tardy DC (1999) J Phys Chem A 103:8433–8439
7. Tsang W, Hampson RF (1986) J Phys Chem Ref Data 15:1087
8. Mebel AM, Diau EWG, Lin MC, Morokuma K (1996) J Am Chem Soc 118:9759–9771
9. Benson SW (1994) Int J Chem Kinet 26:997–1011
10. Heinemann P, Hofmann-Sievert R, Hoyermann K (1988) Symp Int Combust Proc 21:865
11. Scherzer K, Loser U, Stiller W (1987) Z Chem 27:300
12. Miller WH (1979) J Am Chem Soc 101:6810
13. Truhlar DG, Garrett BC (1987) J Chem Phys 84:365
14. Truhlar DG, Garrett BC, Klippenstein SJ (1996) J Phys Chem 100:12771
15. Truhlar DG, Garrett BC (1984) Annu Rev Phys Chem 35:159
16. Hase W (1998) Acc Chem Res 31:659
17. Truhlar DG, Gordon MS (1990) Science 249:491
18. Truong TN, Truhlar DG (1990) J Chem Phys 93:1761
19. Frisch MJ, Trucks GW, Schlegel HB, Scuseria GE, Robb MA, Cheeseman JR, Zakrzewski VG, Montgomery JA, Stratmann RE, Burant JC, Dapprich S, Daniels AD, Kudin KN, Strain MC, Farkas O, Tomasi J, Barone V, Cossi M, Cammi R, Mennucci B, Pomelli C, Adamo C, Clifford S, Ochterski J, Peterson GA, Ayala PY, Cui Q, Morokuma K, Malik DK, Rabuk AD, Raghavachari K, Foresman JB, Cioslowski J, Ortiz JV, Stefanov BB, Liu G, Liashenko A, Piskorz P, Komaromi I, Gomperts R, Martin RL, Fox DJ,

Keith T, Al-Laham MA, Peng CY, Nanayakkara A, Gonzalez C, Chalacombe M, Gill PMW, Johnson BG, Chen W, Wong MW, Andres JL, Head-Gordon M, Replogle ES, Pople JA (1998) Gaussian 98. Gaussian, Pittsburgh, PA
20. Frisch MJ, Head-Gordon M, Pople JA (1990) Chem Phys Lett 166:275
21. Peterson KA, Woon DE, Dunning TH (1994) J Chem Phys 100: 7410
22. Woon DE, Dunning TH (1993) J Chem Phys 98:1358
23. Pople JA, Head-Gordon M, Raghavachari K (1987) J Chem Phys 87:5968
24. Gonzalez C, Schlegel HB (1989) J Chem Phys 90:2154
25. Chuang YY et al (1999) Polyrate, Program vision 8.2, Minneapolis
26. Kaye GWC, Laby TH (1995) Tables of physical and chemical constants, Longman, London
27. Duncan JL (1974) Mol Phys 28:1177
28. Shimanouchi T (1972) Tables of molecular vibrational frequencies consolidated. National Bureau of Standards
29. Ira NL (1975) Molecular spectroscopy, Wiley, New York
30. Fahr A, Laufer AH, Tardy DC (1988) J Phys Chem 92:7229
31. Chase MW Jr (1998) NIST-JANAF thermochemical tables. J Phys Chem Ref Data, Monograph 9, pp 11747–14502